Statistical assessment of order within systems of nanoparticles: Determining the efficacy of patterned substrates to facilitate ordering within nanoparticle monolayers fabricated through electrophoretic deposition

Alex J. Krejci,[1,2] Colin G. W. Thomas,[1,2] and James H. Dickerson[1,2,3,*]

[1]*Department of Physics and Astronomy, Vanderbilt University, Nashville, Tennessee, 37235, USA*

[2]*Vanderbilt Institute for Nanoscale Science and Engineering, Vanderbilt University, Nashville, Tennessee, 37235, USA*

[3]*Department of Chemistry, Vanderbilt University, Nashville, Tennessee, 37235, USA*

(Received 8 January 2013; published 18 April 2013)

The degree of order within nanoparticle monolayers deposited through electrophoretic deposition on lithographically patterned and unpatterned substrates was analyzed using four complementary measures of order: Voronoi-cell edge-fraction entropy, local bond-orientation order parameter, translational order parameter, and anisotropy order parameter. From these measures of order, we determined that the pattern had an influence on some aspects of the ordering within the nanoparticle monolayer but had no effect on others. The Voronoi-cell edge-fraction entropy did not measurably change due to the pattern, indicating that the pattern has no effect on the number of defects present. The translational order parameter also had no change due to the pattern. The local bond-orientation order parameter had a measurable change, indicating the pattern increased the bond ordering slightly. Also, the anisotropy order parameter developed herein indicated an increase in order. The direction of the increased order corresponded with the direction of the anisotropy designed on the patterned substrate, strongly suggesting that the pattern drives the particles to become more ordered.

DOI: 10.1103/PhysRevE.87.042307 PACS number(s): 81.16.Dn, 68.37.Hk, 81.07.−b, 78.67.Bf

I. INTRODUCTION

Ordered systems of nanoparticles (supercrystals) have attracted significant interest recently because of the many potential applications resulting from the unique behaviors of these arrangements of nanoparticles (NPs) [1–6]. Supercrystals can be fabricated using a variety of techniques, such as evaporative self-assembly, Langmuir-Blodgett, and ligand-mediated self-assembly [2,7–13]. However, if supercrystals are to be employed in applications on an industrial scale, alternative techniques that are more rapid and easily scalable should be considered. Recently, we have developed such a rapid and scalable alternative using electrophoretic deposition (EPD). We have demonstrated the potential of EPD in creating two-dimensional nanoparticle films (NP monolayers). However, these films display only local ordering. If order can be enhanced, EPD can rival the aforementioned techniques in the production of supercrystals [14–16]. To enhance ordering within the films, we must initially understand the mechanisms behind ordering. The mechanisms can be more easily explored if we first have tools with which to quantify the order. For example, measuring variations in the degree of order as a result of changes in electric field strength, substrate material, suspension concentration, etc., would give insights into the mechanisms behind ordering.

Quantifying order has been explored in many fields, including biology, material science, chemistry, physics, and mathematics, among others [17–22]. These explorations confirm that order can be quantified on an absolution scale (complete order, corresponding to an ideal crystal, to complete disorder, corresponding to an ideal gas). The entire scale of order can be represented by order parameters that range from one (complete order) to zero (complete disorder). We have adopted three complementary, statistical measures of order that can be applied to any system of particles in two dimensions (2D) (including the EPD films). In addition, we have employed a measure of order that detects anisotropy of ordering within a system that utilizes a complex order parameter. All four of these measures have three-dimensional analogs.

Herein, we describe an attempt to improve ordering with NP monolayers fabricated by EPD. During NP film fabrication using EPD, local ordering can occur [16]; however, long-range ordering in EPD can be inhibited because of two properties. First, in a typical deposition, the film simultaneously grows in different regions throughout the substrate as particles deposit individually on the surface. Second, when using a flat electrode, no asymmetry exists in the plane of the electrode; therefore, ordering in this plane will have no preferential direction. The combination of simultaneous, localized, supercrystal nucleation and substrate symmetry inhibit the creation of films with long-range order.

Since the basic EPD process cannot facilitate long-range ordering, we consider modifications to the process. One possible way to do this is to create a patterned substrate that creates predefined locations for each particle. This approach has been successfully implemented in other liquid phase assembly approaches such as polymer-mediated assembly and evaporation self-assembly [23–28]. In this paper, we fabricated nanopatterned substrates with sixfold symmetry, which introduced long-range periodicity and anisotropy into the system to facilitate ordering. EPD was used to deposit nanoparticles on these substrates. Scanning electron microscopy (SEM) was used to image individual NPs on the substrate surface. The images were then analyzed to identify and locate particles on the substrate, resulting in a list of particle locations. This list was then distilled into four statistical quantities that were employed to compare the degree of order between patterned and unpatterned substrates.

*james.dickerson@vanderbilt.edu

II. EXPERIMENT

Patterned substrates were created by spin coating hydrogen silsesquioxane (HSQ) (Fox-12, Dow Corning) onto epi-ready, phosphorus-doped, silicon wafers (n-type MEMC Electronic Materials SDN) with an extant native oxide surface layer. After spin coating, the substrate was immediately baked on a hot plate at 90 °C for 40 min. The film was then exposed to electron-beam radiation using a Raith e-Line electron-beam lithography instrument. Tetramethylammonium hydroxide (TMAH) heated to 55 °C was used to develop the exposed film [29,30]. The resulting substrate contained both patterned and unpatterned regions; the unpatterned regions were used as a control reference for our measures of ordering. The patterns were composed of rectangular line features of length 60 ± 2 nm and width of 20 ± 2 nm, written in a hexagonal lattice configuration with a pitch equal to the line length (see Fig. S1 in Supplemental Material) [31].

NPs of iron oxide (FeO/Fe_3O_4) were synthesized by thermal decomposition of iron oleate in the presence of oleic acid using 1-octadecene as a solvent (adapted from Park *et al.*) [16,32,33]. The spherical, synthesized nanoparticles were measured to possess a diameter of 9.6 ± 0.9 nm by using a Philips CM20 transmission electron microscope. The synthesized particles were cleaned through centrifugation and resuspended in hexane at a concentration of ∼0.1 mg/mL. EPD was performed by first mounting, in parallel pate configuration, two electrodes with a 5.0-mm gap. The patterned substrate acted as the negative electrode and an unprocessed silicon wafer as the positive electrode. The wafers (each being ∼1.5 cm × 1.5 cm in area) were then inserted into the NP suspension, after which, a 500-V potential was applied across the gap for 15 s. The voltage was turned off, the electrodes extracted, and the voltage reapplied for 1 min. The resulting NP film on the patterned substrate was imaged using backscatter electron detection on the Raith e-Line operating in scanning electron microscopy mode. At least five SEM images, each representing >900 nm × 600 nm regions, taken from both the patterned and the unpatterned regions, were used in the determination of the Voronoi entropy and the local order parameter. The figures, presented in the main body of this article, show only a small section of a single SEM image; for an entire SEM image, refer to Fig. S2 [31].

III. DISCUSSION AND RESULTS

Before any measures of order were made, we needed to process the images in order to identify and locate the particles within the images. As voids and pattern elements existed within the films, we needed to locate these features and to treat particles neighboring these features as boundary particles. After image processing, we located all the particles and analyzed the order using four measures. First, we found the informational entropy relating to the number of edges for the Voronoi cells [34–37]. Next, we calculated the local bond-orientational order parameter (ψ) and the translational order parameter (τ) [38–43]. Two NPs are considered *bonded* if they share a Voronoi edge. The nature of the bonding (physical, chemical) is not important for the statistical analysis of the ordering. Finally, we developed the anisotropy order parameter, which is similar to the global bond-orientational order parameter, and demonstrated its practicability [42,44].

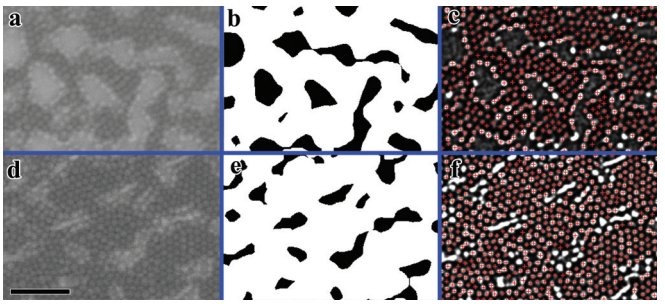

FIG. 1. (Color) (a) SEM image of iron oxide NPs on unpatterned region of substrate. (b) A segmented image of (a), with black areas representing voids in the film. (c) A processed version of (a), optimized for identification of particle locations. Identified particles are marked by red (gray) plus signs. (d)–(f) Corresponding images for the patterned substrates. (e) In this example, black regions represent both voids and pattern elements. (Scale bar = 100 nm.)

A. Image preparation

To assess order, one must measure how the location of one particle relates to the location of other particles. In particular, a particle's location relative to said particle's *nearest neighbors* is vital for measuring order. Different techniques exist for determining nearest neighbors; in this work, we utilize the two-dimensional Voronoi tessellation for each image to determine neighbors [15,34,45,46]. Two Voronoi cells that share an edge are considered neighbors, and the NPs that are represented by the cells are considered *bonded*. In a portion of our sample images, regions exist in which no particles have deposited [identified as either voids or pattern elements, hereafter referred to simply as *voids*; Figs. 1(a), and 1(c)]. Since the Voronoi tessellation is a space-filling pattern designation, particles that deposited next to these voids will appear to have neighbors on the side facing the void. Such a miscount of the number of neighbors can have deleterious effects on the measure of ordering; thus, we modified our Voronoi tessellation assessment by removing from the tessellation any Voronoi cell that contained one or more vertices that were adjacent to either void. Additionally, we removed particles on the edge of the image (border particles) from the measurement. Border particles are identified as those having a Voronoi vertex at $\pm\infty$. Thus, we regarded all particles that neighbor a void and all particles at the edge of the image as boundary particles. All particles identified as boundary particles are disregarded in all further analyses. In the following discussion, we first address how to segregate each image into two regions: one consisting of voids, one consisting of regions with NP deposition. Then, we discuss how to identify the location of each particle within an image, a necessary input for obtaining the desired statistical measures.

1. Image segmentation

The locations of voids and pattern elements were recorded by segmenting the original image into a black and white image, where black indicated voids and pattern elements in

the film and white indicated regions where particles had deposited. The segmentation of the image was done by applying a series of image processing filters. First, a series of filters [median, Gaussian blur (low pass), and high pass] were applied. Median filters are nonlinear filters that address a single pixel and replace said pixel by the median value in a $N \times M$ neighborhood (kernel) surrounding said pixel. Median filters are very effective at removing impulse noise (isolated noise spikes) while preserving high frequency detail (edges). A Gaussian blur is a low pass filter that attenuates high frequency data while passing low frequency data. For the purposes of segmentation, individual particles are not important; rather the region that is occupied by particles is of interest. Thus, we applied a Gaussian blur so that the particle edge data are lost, and the particles became indistinguishable. High pass filters act in a manner opposite to low pass filters, attenuating low frequencies and passing high frequencies within the data. In this way, very low frequency data that do not give information of the location of particles can be removed. In this case, the desired effect of the high pass filter is to make the average intensity uniform throughout the image (leveling). Next, a series of contrast adjustments and image multiplications (multiplying the image by itself in this case) were applied, with the final contrast adjustment creating a black and white image. The image was inverted so that the voids and pattern elements appeared black. Then, a maximum or minimum morphological operation was used to make minor adjustments to the size of the segmented regions [Figs. 1(b) and 1(d)]. Figure S2 shows the sequence of images after applying each filter [31]. One aspect of this technique worth noting is that the blur of the Gaussian filter limited the size of the void that could be detected. Thus, smaller voids will be blended in with the particles and be seen as regions with particles. To verify the efficacy of this procedure, the resulting segmented image is multiplied by the original image, and visual inspection by side-by-side comparison of the result and the original image is performed.

2. *Particle location measurement*

To identify particles in each image, we again applied a series of filters to the original SEM images. First, a median filter was used to remove impulse noise. A high pass filter was used to level the image while maintaining the definition of each particle. A Gaussian filter was applied to remove noise over an individual particle and to create an intensity peak at the center of the particle while maintaining the definition of each particle. After this, a series of contrast adjustments and image multiplications were applied to amplify the contrast between the particles and the background. The particles were then identified first by using MATLAB'S *imregionalmax* function, which finds the regional maxima within an image, and then by finding the centroid of each identified region. After finding the particles' locations, a marker (red plus) was drawn at each particle location. The images were then visually inspected to ensure that the center of each particle was located (Fig. S3 shows a sequence of images after each filter) [31].

The list of identified particle locations was then compared to the segmented image. Any particles that have been located within a void or pattern element regions are removed from the list. Any identified particles that lie on the border of the image were removed from the list, as they either did not identify actual particles or did not accurately reflect the location of an actual particle, since the center of the particle may have lain outside the border of the image. Finally, only uniquely identified particle locations were kept. The result was the final list of particle locations, which was used in all further analyses [Figs. 1(c) and 1(f)].

B. Voronoi-cell edge-fraction distribution and entropy

Voronoi tessellations have a long history of use in a variety of fields, including anthropology, astronomy, biology, chemistry, computational geometry, physics, and statistics, among others [34,35,45,46]. A Voronoi tessellation, as defined by Okabe, is an association, ". . .given a set of two or more but a finite number of distinct points in the Euclidean plane, . . ." of ". . .all locations in that space with the closest member(s) of the point set with respect to the Euclidean distance" [46]. The Voronoi tessellation supplies a great deal of information, a few examples of which are listed below:

(i) First, the Voronoi tessellation provides a visual tool that could be used.

(ii) The fraction of Voronoi cells with n sides ($n = 3 - 9$) can be extracted, giving a one-dimensional (1D) set of data. If ordering exists within the system, these data will allow for the identification of the symmetry of the order (in 2D, either fourfold or sixfold symmetry can exist as a space-filling symmetry).

(iii) Informational entropy can be calculated from the 1D Voronoi-cell edge-fraction distribution data set, giving 0D data.

(iv) Next, nearest neighbors in two dimensions can be defined in multiple ways. One common definition is two particles that share a Voronoi edge. We used this definition and consider these nearest neighbors to be bonded—integral information in the calculation of two of the following statistical measures of order.

(v) The Voronoi tessellation is used to discover which particles are at a boundary of a void or a border of the image. These particles should be excluded from certain measurements.

(vi) The Voronoi tessellation can be used to calculate the average particle-particle spacing between nearest neighbors for well-packed particles [15].

(vii) The Voronoi-cell edge can be used to calculate bond angles between nearest neighbors.

(viii) Furthermore, the Voronoi tessellation allows one to quantitatively define a hexagonally packed particle as shown in Sec. IV below.

Seven of the eight above pieces of information extracted from the Voronoi tessellation will be utilized. Given the list of particle locations found in Sec. I, a Voronoi diagram was constructed (Figs. 2(a) and 2(b); larger images are supplied in Fig. S2 [31]). Using the Voronoi diagram, a distribution of the fraction of Voronoi cells with n ($n = 3 - 9$) edges was plotted. This distribution, shown in Fig. 2(c), was created by averaging over at least five images for regions with and without a pattern. The error bars were determined by taking

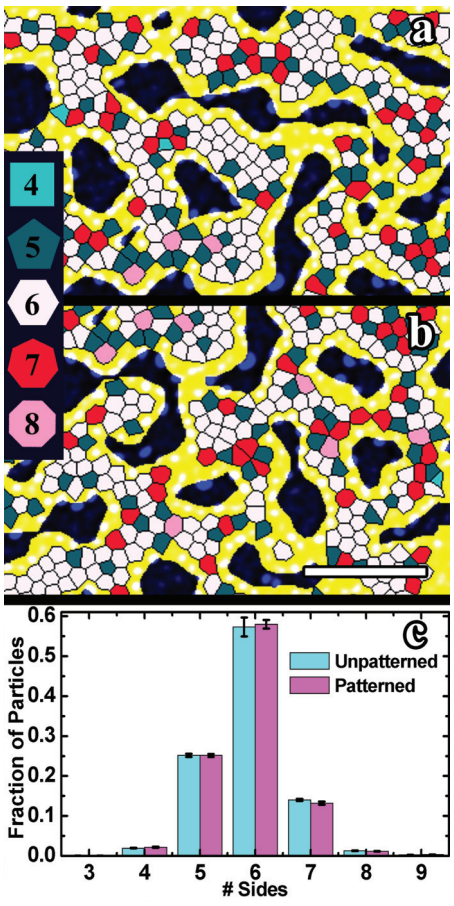

FIG. 2. (Color) (a) and (b) Voronoi tessellation, derived from an image of a nanoparticle film shown in Figs. 1(c) and 1(f). Voronoi cells with one or more vertices within a black region of the segmented images [Figs. 1(b) and 1(e)] were removed. Cells were color coded based on the number of sides of the cell. No cells with greater than 8 or less than 4 sides were shown. (c) Histogram showing the fraction of particles with n sides, where $n = 3 - 9$. Within error, the unpatterned and patterned substrates were equivalent. (Scale bar = 100 nm.)

the standard deviations of the percentages from the patterned and unpatterned substrates, respectively.

From Fig. 2(c), a clear peak was observed at $n = 6$, indicating the particles tended to pack hexagonally. Such hexagonal ordering can be clearly seen in the original SEM. The histogram confirmed that the distribution for the patterned and unpatterned substrates is measurably the same. Finally, we calculated the informational entropy, S, from this distribution using

$$S = -\sum_{i=3}^{9} p_i \ln p_i, \tag{1}$$

where p_i is the probability of a Voronoi cell having i edges [15,36,47]. The entropy provides a direct numerical comparison between the data in the distribution. The entropy was $S = 1.05 \pm 0.03$ for the patterned substrate and $S = 1.10 \pm 0.03$ for the unpatterned substrates. The entropy was measurably the same for both the patterned and unpatterned substrate, concurring with what was observed in the distribution graph. Thus, the presence of a pattern did not significantly affect the Voronoi-cell edge-fraction distribution, indicating that the pattern had not reduced the fraction of defects present within the film. Despite this, the pattern still could affect other measures of order.

C. Order parameters—local bond-orientational order parameter and translational order parameter

The use of order parameters has been heavily advocated by Torquato, Truskett, and Kansal in a number of publications [38,40,42,48]. Order parameters are numbers that describe the order of a system such that a system with complete disorder will have an order parameter of zero and one with complete order will have an order parameter equal to 1. Torquato, Truskett, and Kansal have gone further to demonstrate that by measuring two order parameters, one can create an order-parameter space, which illustrates the relative placement of fluid, glassy, and crystal equilibrium structures [38,40]. Adopting these ideas, we measured two order parameters, the bond-orientational order parameter and the translation order parameter.

The bond-orientational order parameter is calculated for a Voronoi tessellation, by extracting only those Voronoi cells with no vertices at $\pm\infty$ and no vertices in a void. For each cell, the local bond-orientational order parameter, $\psi_{6,\mathrm{local}}$, was calculated for each particle.

$$\begin{aligned} \psi_{jn}^{\zeta} &= e^{i\zeta\theta_{jn}}, \\ \psi_{\zeta,\mathrm{local}} &= \frac{1}{N_n}\sum_{j=1}^{N_n}\psi_{jn}^{\zeta}, \end{aligned} \tag{2}$$

where ζ is the periodicity [$\zeta = 6$ represents hexagonal, close packing as seen in Fig. 2(c)]; θ_{jn} is the bond angle j for bonds emanating from particle n measured relative to an arbitrary, fixed axis; and N_n is the number of neighbors of particle n [43]. The distribution of $\psi_{6,\mathrm{local}}$ is plotted for all particles averaged over all images for patterned and unpatterned regions of film (Fig. 3). $\psi_{6,\mathrm{local}}$ was found for each particle in a single image; then the discrete instances of $\psi_{6,\mathrm{local}}$ were binned. The bins were normalized so that they indicated the percentage of particles having a range of $\psi_{6,\mathrm{local}}$ represented by the bin. The average value was calculated by separately averaging each bin over all images of patterned and unpatterned substrates. Error bars are calculated for each bin by taking the standard deviation from all images of patterned or unpatterned substrates. The distribution for the patterned substrate was shifted to the right relative to the unpatterned substrate, indicating that local particle ordering was enhanced when the pattern was present. Thereafter, the average $\psi_{6,\mathrm{local}}$ over all particles in a single image was calculated. Subsequently, the average was determined over all of the images of the patterned and unpatterned substrates, separately. The error in $\psi_{6,\mathrm{local}}$ was calculated by taking the standard deviation of the average value from all images. For the patterned substrate $\psi_{6,\mathrm{local}}$ was 0.522 ± 0.013, and for the unpatterned substrate the value was 0.490 ± 0.013.

Given the plot of the $\psi_{6,\mathrm{local}}$ distribution and the values themselves, patterning slightly increased the degree of bond-orientational order within the system. However, the Voronoi-cell edge-fraction distribution and corresponding entropy

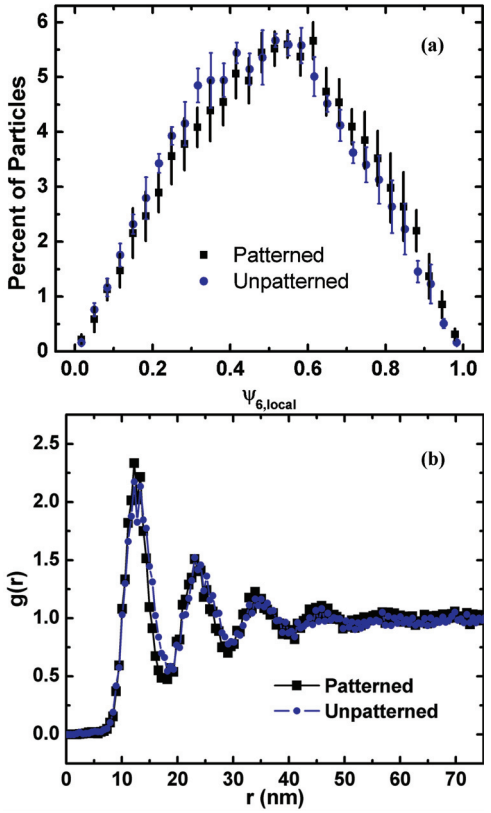

FIG. 3. (Color) (a) Distribution of $\psi_{6,\text{local}}$ values for patterned and unpatterned regions. The patterned substrate distribution was shifted slightly to the right, indicating a greater degree of local ordering. (b) Pair correlation function which is used to calculate τ, the translational order parameter.

measured for the patterned and unpatterned substrates were equivalent. Note that a particle with a six-sided Voronoi cell may not be truly hexagonally packed. Further, a six-sided Voronoi cell can evolve from a hexagonally packed NP array that possesses small deviations from ideal hexagonal packing. The discrepancy between the two measures of order is likely due to one of the two aforementioned causes.

Next, we measure the translational order parameter, τ, defined as

$$\tau = \frac{1}{r_c}\int_0^{r_c} |g(r) - 1| dr, \tag{3}$$

where $g(r)$ is the 2D pair correlation function, and r_c is the maximum radius measured in the pair correlation function [40]. This translational order parameter does not depend on the symmetry of the system. Additionally, the presence of voids does not affect the measure due to the normalization of $g(r)$ by the density of particles. Figure 3(b) shows $g(r)$, averaged over all images for the patterned and unpatterned substrates. $g(r)$ was very similar for substrates with and without patterning. Using the values for $g(r)$ shown in Fig. 3(b), τ was calculated. r_c was set to 76 nm, as $g(r) \sim 1$ for this value of r_c. Values for $g(r)$ at $r > 76$ nm have little effect on τ. The results of the calculations, averaged over multiple images, are $\tau = 0.257 \pm 0.010$ for the patterned substrates and $\tau = 0.250 \pm 0.005$ for unpatterned substrates. Again, uncertainties were calculated by taking the standard deviation of values measured from five or more images.

While the bond-orientation order parameter indicates some increase in ordering for the patterned substrate, the translational order parameters were equivalent for the patterned and unpatterned substrates. Comparing these results to the order parameter phase space, as described in Truskett *et al.*, our analyzed systems fell closest to the glassy regime [40]. In Truskett *et al.*, the translational order parameter was not observed to be as sensitive as the bond-orientational order parameter when ensembles resided in the glassy regime. This could explain why no significant difference in translational order was measured, while a small difference for bond-orientation order was observed.

D. Anisotropy complex order parameter

The anisotropy complex orderparameter is designed to detect global anisotropy in the direction of bond between two particles. This anisotropy can be visualized by the angular orientation of hexagonal Voronoi cells (Fig. S4) [31]. Importantly, the anisotropy measured here is not designed to ascertain the symmetry of a Voronoi cell. Anisotropy in the bond direction could be introduced by adding a physical anisotropy into the system (e.g., a unidirectional magnetic field, a nonradial fluid flow, anisotropic geometry, etc.). In such cases, NPs can still pack hexagonally; however, neighbors prefer to pack in particular directions relative to the physical anisotropy.

However, the measurement of anisotropy in the bond direction should be dealt with carefully. A measurement that is taken within a region that is smaller than the correlation length of the system will surely display a high degree of anisotropy since all the particles are correlated. In this case, we are interested in how the bond directions within the uncorrelated regions relate to each other.

1. Techniques and characteristics of anisotropy measurement

The degree of anisotropy in the system was measured using a modification of the global bond-orientational order parameter,

$$\begin{aligned} \psi_{jn}^{\zeta} &= e^{i\zeta\theta_{jn}}, \\ \psi_{6,\text{global}} &= \frac{1}{N_\zeta}\sum_{j=1}^{N_\zeta}\sum_{n=1}^{\zeta}\frac{\psi_{jn}^{6}}{\zeta}, \\ \Psi_{\text{an}} &= \|\psi_{6,\text{global}}\|, \\ \Theta_{\text{an}} &= \arctan\left[\frac{\text{Im}(\psi_{6,\text{global}})}{\text{Re}(\psi_{6,\text{global}})}\right]. \end{aligned} \tag{4}$$

This value is very similar to $\psi_{6,\text{local}}$; however, the average is taken over all bonds in a film of particles rather than over bonds for a single particle, then over all particles [42]. At this point, Ψ_{an} is equivalent to the global bond-orientation order parameter. Yet, because we were interested in the direction of the ordering of particles, we only included particles that were *well ordered*, that is, *hexagonally packed*. We defined a particle to be *hexagonally packed* if the particle met two conditions:

(i) The number of sides of the particle's corresponding Voronoi cell matched the peak periodicity of ordering for the system (e.g., six for hexagonal close packing).

(ii) All edge lengths of the corresponding Voronoi cell were within 60% of the median edge length of the cell. Visual inspection shows that this condition works well to choose only hexagonally packed particles.

Before applying this measure to the NP samples, we should first understand the behavior of characteristics of Ψ_{an}. To understand these characteristics we first observed how Ψ_{an} changed as a function of the standard deviation of a set of oriented bonds. Thus, we calculated Ψ_{an} using 100 000 randomly generated angles that followed a Gaussian distribution. The standard deviation of the distribution was varied, and a plot of Ψ_{an} versus the standard deviation was generated [Fig. 4(a)]. We also plotted the derivative of the standard deviation curve (averaged over 12 points for smoothing), which indicated the sensitivity of Ψ_{an} to changes in the standard deviation. As evinced from the plot, above a standard deviation of 50% of the total angular domain, the order parameter was nearly zero. This effect caused measured values of Ψ_{an} to be less than expected for the ideal case, as seen in Sec. III D2.

Another important characteristic of Ψ_{an} was how the quantity varied with sample size. In a real system, the sample size can be related to the correlation length of the system, as discussed in Sec. III D2. For modeling Ψ_{an}, we assume that each correlated region contains perfectly oriented bonds and that each region is equal in size. Thus, for each correlated region, we simulate one random angle.

Figure 4(b) shows how the value of Ψ_{an} changes with sampling size. The values were simulated by the following method:

(i) An integer number of random angles between 0 and $\pi/3$ were generated. Then, a number of angles was taken as the sample size;

(ii) Ψ_{an} was calculated based on the random angles;

(iii) Steps 1 and 2 were repeated 10 000 times for each sample size; the mean and standard deviation (σ) were calculated for the set;

(iv) Steps 1–3 were repeated using all integers in the range (1–800) for the sample size.

From Fig. 4(b), the mean value of Ψ_{an} was 1 for a sample size of 1, which was expected as all bond angles were perfectly aligned. Interestingly, for $\Psi_{an} = 1$ to have been known with a 95.4% (2σ) confidence level (that is, a 95.4% probability that the result was not a random event), the measured samples size must have been $S_s \gtrsim 4$. Further, for 99.7% (3σ) confidence level a measured sample size of $\gtrsim$5 was required. The inset of Fig. 2(b) provides a histogram of the 10 000 Ψ_{an} values for a sample size of 600. The NP samples analyzed here consist of approximately 600 constituents; thus, we simulated up to 800 to account for all probable quantities. We expected simulations that comprised a sample size larger than 800 to follow the trend observed in Fig. 2(b).

These characterizations are important for determining the necessary quality and sample size of data to obtain a meaningful result. However, a *background measurement* is also vital to determine if anisotropy existed. We obtained *background values* by amassing a database of angles of bonds from all

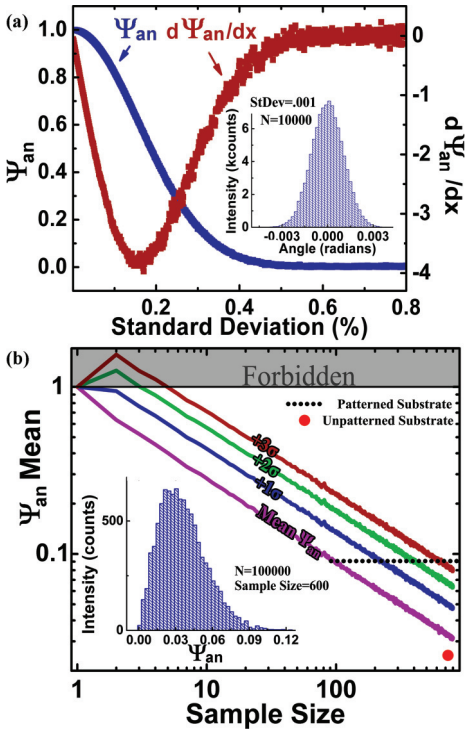

FIG. 4. (Color) The properties of Ψ_{an} as determined by simulating a set of bond angles (a) The blue (dark) line demonstrates how Ψ_{an} varies as the standard deviation of bond angles varies. The standard deviation is plotted in percent of total angular range. The red (light) line shows the derivative of Ψ_{an} as a function of the standard deviation, indicating the sensitivity of Ψ_{an} to changes in the standard deviation. The inset is an example of simulated bond angles for a set of bond angles with a 0.001% standard deviation and an angular range of 2π. (b) This graph demonstrates that even for completely disordered systems, Ψ_{an} will not be zero and will depend on the sample size. The sample size is a measure of the number of simulated correlated regions. Each correlated region is randomly oriented, and all bonds within a single correlated region are equivalent. Ψ_{an} is calculated 100 000 at each simulated sample size. The $+1\sigma$, $+2\sigma$, and $+3\sigma$ lines indicate the mean value of Ψ_{an} plus 1, 2, and 3 times the standard deviation of the 100 000 calculated values. The red (light gray), individual dot represents the value measured for the unpatterned substrate. The dot lies below the mean Ψ_{an}, which is expected since Ψ_{an} is simulated for perfect hexagons. The black dotted line lies along the value measured for the patterned substrate. The sample size for the patterned substrate is well beyond the edge of the simulation at 2180. Thus, the patterned substrate is well above the $+3\sigma$ line. The gray region (top) is forbidden because mathematically, Ψ_{an} cannot exceed 1. The inset shows a histogram of 100 000 Ψ_{an} values simulated for a sample size of 600.

the particles in a reference unpatterned image. The database comprised seven columns—six for the bond angles for each particle that matched the aforementioned selection criteria and one for the area of the Voronoi cell. The *background value* was obtained by calculating Ψ_{an} for a set of randomly selected rows of angles within the database for which the sum of the area from each row was approximately equal to the total area of the selected Voronoi cells in the original image. The calculation was repeated 1000 times, using a different, randomly selected row of angles each time, and the mean was used as the

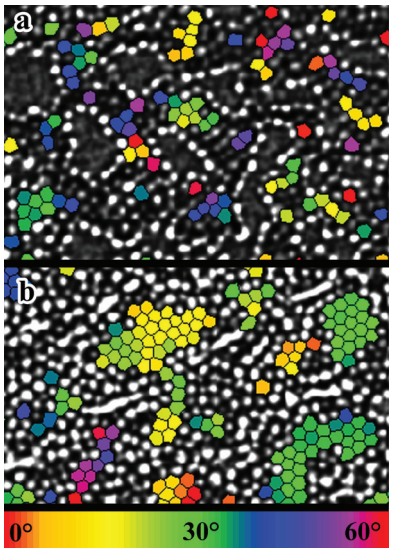

FIG. 5. (Color) A subset of the Voronoi cells from Fig. 2 having six sides and all edge lengths within 60% of the median edge length for (a) unpatterned regions and (b) patterned regions. The color indicates the circular mean (over the range 0°–60°) of the six bond angles for each cell.

background value. This method was tested on unpatterned images to determine its effectiveness. The resulting Ψ_{an} and the *background value* were equivalent within uncertainty for the images of unpatterned regions.

2. *Measurement on patterned substrate*

With the measurement techniques and characteristics established for Ψ_{an}, we calculated Ψ_{an} for nanoparticle monolayers on the patterned substrate and unpatterned substrate. The subset of Voronoi cells that fit the selection criteria is shown in Figs. 5(a) and 5(b) for the unpatterned and patterned substrate, respectively. Here, the color of each Voronoi cell was determined by the circular average, over the range (0°–60°) of all of the six bond directions. The anisotropy order parameter for the unpatterned substrate was $\Psi_{an} = 0.021 \pm .007$; the order parameter for the patterned substrate was calculated to be $\Psi_{an} = 0.089 \pm .004$. The associated error in Ψ_{an} was calculated by varying the measured x and y positions of each particle's location by a random amount between ± 0.5 pixels. This was repeated 1000 times. Ψ_{an} was found by taking the mean and the error was found by taking the standard deviation of the 1000 measurements. A *background value* was calculated (using the aforementioned method) to be 0.033 ± 0.015 for the unpatterned substrate and 0.029 ± 0.011 for the patterned substrate. These values strongly suggest the existence of anisotropy in bonding due to the anisotropic geometry of the pattern.

In the following, we demonstrate how we determined the sample size of the data in terms of the number of correlated regions. We compared the value of Ψ_{an} for the obtained sample sizes to the simulated data to ensure that our sample size was sufficiently large. To find the sample size, we first calculated the correlation length, ξ_c, of a system, as determined from the following:

$$g_6(r) = \langle \cos[6(\theta_i - \theta_0)] \rangle \sim e^{-r/\xi_c}, \tag{5}$$

where $g_6(r)$ is the bond-orientation correlation function, which was measured from the bonds between two nearest neighbor particles [41,49]. Each bond position was defined at the midpoint of the bond, r_0; the bond angle, θ_0, was measured relative to a fixed, arbitrary axis. The brackets represented a numerical average over all bonds i lying in an annular ring at $r \pm \Delta r$. This measurement was repeated using each bond that lay farther than r_{max} from the edge of the sampling region, where r_{max} was the maximum measured radius for $g_6(r)$. We use 0.25 nm for Δr and 40 nm for r_{max}. The mean value of $g_6(r)$ is similar to the mean value of the $\psi_{6,global}$. The major distinction between the two parameters lies in the fact that in the global bond-orientational order parameter, each bond is treated with equal weight. In the mean of the bond-orientation correlation function, each annular region is weighted equally. The sample size, S_s, was then calculated to be

$$S_s = \frac{A_s}{\pi \xi_c^2}, \tag{6}$$

where A_s is the area of the sampled Voronoi cells, and $\pi \xi_c^2$ is the area of a single sample. For the patterned substrate, the sample size was 2180; for the unpatterned substrate, the sample size was 764. For the patterned substrate, the sample size is much larger than the region simulated; however, the value of the anisotropy is clearly more than three standard deviations above the simulated mean. For the unpatterned substrate, the value lies below the mean simulated value [Fig. 4(b)]. This was expected as the simulation assumes that each correlated region only represents perfectly hexagonally packed NPs. Figure 4(a) shows that any variation from perfect hexagonal packing will decrease the value of Ψ_{an}. Given this and the comparison to the background measurement, we are confident that anisotropy in ordering exists in our systems. While the order parameter indicated the existence of anisotropy on the patterned substrate, some possibility exists that this anisotropy that we detected was not caused by the pattern. To corroborate the conjecture that the patterned substrate was the primary driver of ordering, the direction of anisotropy, as measured by the complex order parameter, $\Theta_{an}/6$, was compared with the direction of the patterned lines. Θ_{an} was divided by 6 because the system's sixfold symmetry limited the angular range for the bond angles to $2\pi/6$. The patterned lines were measured to be at $25° \pm 3°$. The mean and standard deviation of $\Theta_{an}/6$ were found using the same method for calculating the mean and standard deviation of Θ_{an}, resulting in $\Theta_{an}/6 = 21.8° \pm 0.5°$. To verify this result, we also plotted a histogram of the measured angles. We expected the distribution of angles to reflect a Gaussian distribution with circular symmetry. The von Mises distribution can be used as a circular analog to a Gaussian distribution [50,51]. The general form of the von Mises distribution, $P(x)$, is

$$P(x) = \frac{e^{b\cos(x-a)}}{2\pi I_0(b)}, \tag{7}$$

where a is the mean of the distribution, $1/b$ indicates the spread of the distribution, and $I_0(b)$ is a modified Bessel function of the first kind. A total of four fitting parameters

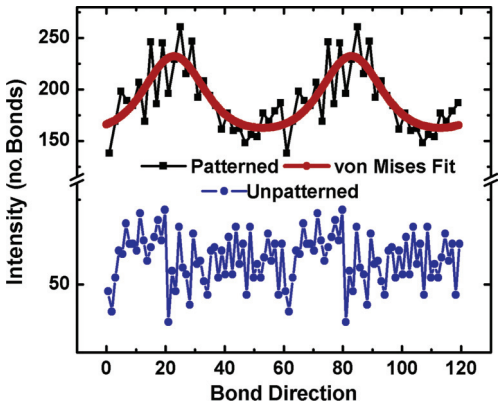

FIG. 6. (Color) The black (square data points) line is the measured number of bonds that are oriented within an angular range, measured relative to the x axis of one of the SEM images of a patterned substrate. The red (light), solid line is a von Mises (circular analog to a normal distribution) fit to the data. Based on the fit, the peak in the distribution occurs at $22.8^\circ \pm 1.3^\circ$, agreeing with the direction of the patterned elements as well as the angle measured by Ψ_{an}. The blue line (lower line with circle data points) shows the equivalent bond-orientation data for the unpatterned substrate.

were employed: (1) a and (2) b as previously described; (3) an additive constant to account for the background signal in the data; and (4) a multiplicative constant as the histogram is not normalized whereas the probability distribution is. The data and the von Mises fit for the patterned substrate and the data for the unpatterned substrate are shown in Fig. 6. Additionally, a more detailed description and results of the fitting are given in the Supplemental Material (Table S1) [31]. The mean value from the von Mises fit, $22.8^\circ \pm 1.3^\circ$, which was obtained from fitting the data in Fig. 6, agreed with the calculated values from both the anisotropy complex order parameter and the direction measures from the image. The anisotropy order parameter indicated that some anisotropy existed in the system beyond that of background noise. That the direction of the anisotropy, as calculated from the anisotropy order parameter and as measured by the distribution of angles, aligns with the direction of the pattern design suggests that the anisotropy in particle ordering is a result of the anisotropy in the pattern design.

IV. CONCLUSIONS

We have successfully measured the degree of order present in NP monolayers fabricated through EPD using three previously developed statistical measures of order, and a measure of order described in this paper. The measures of order were extracted from scanning electron microscope images of the NP monolayers. To apply the statistical measures, we first developed methods to analyze the images. The first method successfully segmented the images into regions with particles and regions without particles. The next method optimized the identification and location of the NPs. Segmentation and particle identification and location then facilitated the acquisition of accurate measures of order within the monolayers. Additionally, we developed a complex order parameter that was used to identify anisotropies in bond orientations. The complex order parameter provided both a magnitude and direction to the order. Characterizations of the order parameter, achieved by simulating bond angles, showed both the importance of the standard deviation of the measurements in a set of oriented bonds and the importance of the sample size relative to the correlation length of the system. Because the sample size had a strong influence on the magnitude of the anisotropy order parameter, we developed a method for obtaining a background measurement.

The four measures of order were applied to NP monolayers deposited on patterned and unpatterned substrates to determine the effect of patterning of order. The pattern was designed with the intention of engendering anisotropy in the bonds between the particles. From the four measures of order, we determined that the pattern did increase ordering within the monolayer. Specifically, the pattern slightly increased the bond-orientational order and engendered anisotropy within the NP bonds. The correlation between the increase in anisotropy, and the pattern characteristics were confirmed by equivalence among the direction of the designed anisotropy and the associated directions measured in the NP bonds. However, the pattern did not increase translational order or reduce the number of defects present.

The four measures of order discussed herein could be applied to assess monolayers deposited under various electrophoretic deposition voltages, external magnetic fields, and on various electrodes to study the effects of these variables on ordering. The measures could also be applied to NP monolayers deposited using other techniques, such as Langmuir-Blodgett and evaporation assisted self-assembly. In future work on three-dimensional nanoparticle crystal growth, techniques such as grazing-incidence small-angle x-ray scattering (GISAXS) could be used to complement the data analysis approaches discussed here. GISAXS can be used to measure order over larger areas than is currently practical using direction imaging. Further, GISAXS can assist in measuring the degree of order in the third dimension, which is not easily analyzed using direct imaging.

ACKNOWLEDGMENTS

The authors would like to thank Charee Peters and Eugenio Victor Garcia for useful discussions on simulations. Thanks also to Hiram Conley and AKM Newaz for useful discussions on electron beam lithography. This research was partially supported by the National Science Foundation, Award No. CAREER DMR-1054161 and by the Army Research Office, Award No. W911NF-12-1-0047. Portions of this work were performed at the Vanderbilt Institute of Nanoscale Science and Engineering, using facilities renovated under NSF Award No. ARI-R2 DMR-0963361. We also acknowledge partial support from the Vanderbilt CLAS Summer Research Award.

[1] A. Courty, J. Richardi, P.-A. Albouy, and M.-P. Pileni, Chem. Mater. **23**, 4186 (2011).

[2] D. V. Talapin, E. V. Shevchenko, C. B. Murray, A. V. Titov, and P. Kral, Nano Lett. **7**, 1213 (2007).

[3] D. V. Talapin and C. B. Murray, Science **310**, 86 (2005).
[4] Z. H. Nie, A. Petukhova, and E. Kumacheva, Nat. Nanotechnol. **5**, 15 (2010).
[5] P. Podsiadlo, G. Krylova, B. Lee, K. Critchley, D. J. Gosztola, D. V. Talapin, P. D. Ashby, and E. V. Shevchenko, J. Am. Chem. Soc. **132**, 8953 (2010).
[6] E. Tam, P. Podsiadlo, E. Shevchenko, D. F. Ogletree, M.-P. Delplancke-Ogletree, and P. D. Ashby, Nano Lett. **10**, 2363 (2010).
[7] A. Ahniyaz, Y. Sakamoto, and L. Bergstrom, Proc. Natl. Acad. Sci. USA **104**, 17570 (2007).
[8] C. Y. Jiang and V. V. Tsukruk, Adv. Mater. **18**, 829 (2006).
[9] F. Kim, S. Kwan, J. Akana, and P. D. Yang, J. Am. Chem. Soc. **123**, 4360 (2001).
[10] C. Salzemann, J. Richardi, I. Lisiecki, J.-J. Weis, and M. P. Pileni, Phys. Rev. Lett. **102**, 144502 (2009).
[11] E. V. Shevchenko, D. V. Talapin, N. A. Kotov, S. O'Brien, and C. B. Murray, Nature **439**, 55 (2006).
[12] K. Yamamoto, C. R. Hogg, S. Yamamuro, T. Hirayama, and S. A. Majetich, Appl. Phys. Lett. **98**, 072509 (2011).
[13] D. Lee, M. F. Rubner, and R. E. Cohen, Nano Lett. **6**, 2305 (2006).
[14] I. Gonzalo-Juan, A. J. Krejci, and J. H. Dickerson, Langmuir **28**, 5295 (2012).
[15] A. J. Krejci, C. G. Thomas, J. Mandal, I. Gonzalo-Juan, W. He, R. L. Stillwell, J. H. Park, D. Prasai, V. Volkov, K. I. Bolotin, and J. H. Dickerson, J. Phys. Chem. B **117**, 1664 (2013).
[16] A. J. Krejci, I. Gonzalo-Juan, and J. H. Dickerson, ACS Appl. Mater. Interfaces **3**, 3611 (2011).
[17] R. Collins and T. Ogawa, Prog. Theor. Phys. **78**, 83 (1987).
[18] H. Kawamura, Prog. Theor. Phys. **61**, 1584 (1979).
[19] A. H. Marcus and S. A. Rice, Phys. Rev. Lett. **77**, 2577 (1996).
[20] N. Meitav and E. N. Ribak, Appl. Phys. Lett. **99**, 221910 (2011).
[21] D. R. Nelson and B. I. Halperin, Phys. Rev. B **19**, 2457 (1979).
[22] P. M. Raj, S. M. Dunn, and W. R. Cannon, J. Comput.-Assist. Microsc. **10**, 33 (1998).
[23] T. P. Bigioni, X. M. Lin, T. T. Nguyen, E. I. Corwin, T. A. Witten, and H. M. Jaeger, Nat. Mater. **5**, 265 (2006).
[24] Y.-J. Oh, C. A. Ross, Y. S. Jung, Y. Wang, and C. V. Thompson, Small **5**, 860 (2009).
[25] J. Rybczynski, U. Ebels, and M. Giersig, Colloids Surf. A **219**, 1 (2003).
[26] R. Shenhar, T. B. Norsten, and V. M. Rotello, Adv. Mater. **17**, 657 (2005).
[27] S. H. Sun, S. Anders, H. F. Hamann, J. U. Thiele, J. E. E. Baglin, T. Thomson, E. E. Fullerton, C. B. Murray, and B. D. Terris, J. Am. Chem. Soc. **124**, 2884 (2002).
[28] C. G. Sztrum, O. Hod, and E. Rabani, J. Phys. Chem. B **109**, 6741 (2005).
[29] S. Choi, M. Yan, L. Wang, and I. Adesida, Microelectron. Eng. **86**, 521 (2009).
[30] I. B. Baek, J. H. Yang, W. J. Cho, C. G. Ahn, K. Im, and S. Lee, J. Vac. Sci. Technol. B **23**, 3120 (2005).
[31] See Supplemental Material at http://link.aps.org/supplemental/10.1103/PhysRevE.87.042307 for images of lithographic patterning, for understanding the anisotropy order parameter, and for fitting parameters for von Mises fitting.
[32] J. Park, K. J. An, Y. S. Hwang, J. G. Park, H. J. Noh, J. Y. Kim, J. H. Park, N. M. Hwang, and T. Hyeon, Nat. Mater. **3**, 891 (2004).
[33] A. J. Krejci, J. Mandal, and J. H. Dickerson, Appl. Phys. Lett. **101**, 043117 (2012).
[34] R. E. Williams, Science **161**, 276 (1968).
[35] P. Richard, J. P. Troadec, L. Oger, and A. Gervois, Phys. Rev. E **63**, 062401 (2001).
[36] R. B. S. Oakeshott and S. F. Edwards, Physica A **189**, 188 (1992).
[37] B. Billia, H. Jamgotchian, and H. N. Thi, Metall. Trans. A **22**, 3041 (1991).
[38] S. Torquato, T. M. Truskett, and P. G. Debenedetti, Phys. Rev. Lett. **84**, 2064 (2000).
[39] A. Panaitescu and A. Kudrolli, Phys. Rev. E **81**, 060301 (2010).
[40] T. M. Truskett, S. Torquato, and P. G. Debenedetti, Phys. Rev. E **62**, 993 (2000).
[41] P. J. Steinhardt, D. R. Nelson, and M. Ronchetti, Phys. Rev. B **28**, 784 (1983).
[42] A. R. Kansal, S. Torquato, and F. H. Stillinger, Phys. Rev. E **66**, 041109 (2002).
[43] B. I. Halperin and D. R. Nelson, Phys. Rev. Lett. **41**, 121 (1978).
[44] H. Weber and D. Marx, Europhys. Lett. **27**, 593 (1994).
[45] F. Aurenhammer, ACM Comput. Surv. **23**, 345 (1991).
[46] A. Okabe, B. Boots, K. Sugihara, and S. N. Chiu, *Spatial Tesselations: Concepts and Applications of Voronoi Diagrams* (John Wiley & Sons Ltd, West Sussex, UK, 2000).
[47] S. Kumar and S. K. Kurtz, Mater. Charact. **31**, 55 (1993).
[48] A. R. Kansal, T. M. Truskett, and S. Torquato, J. Chem. Phys. **113**, 4844 (2000).
[49] D. R. Nelson, Phys. Rev. B **28**, 5515 (1983).
[50] R. Gatto and S. R. Jammalamadaka, Stat. Methodol. **4**, 341 (2007).
[51] C. S. Wallace and D. L. Dowe, Stat. Comput. **10**, 73 (2000).